# Journal of Materials Chemistry A

Accepted Manuscript


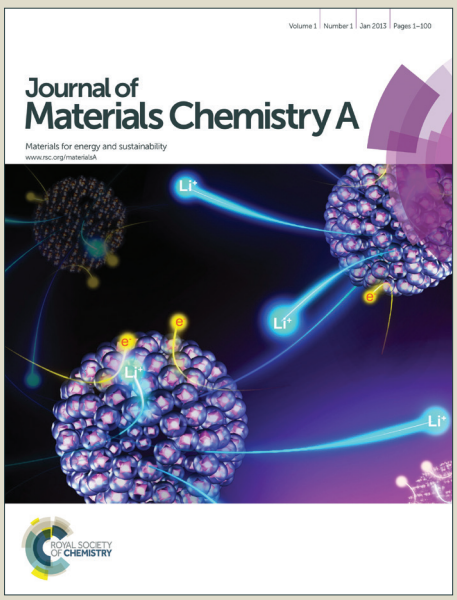





ROYAL SOCIETY OF CHEMISTRY

www.rsc.org/materialsA

Journal of Materials Chemistry A

RSCPublishing

ARTICLE

# *In-situ* Studies of Molecular Packing Dynamics of Bulk-heterojunction Solar Cells induced by the Processing Additive 1-Chloronaphthalene

Cite this: DOI: 10.1039/x0xx00000x

Received 00th January 2012,
Accepted 00th January 2012

DOI: 10.1039/x0xx00000x

www.rsc.org/

Sooncheol Kwon[a,b,†], Jin Kuen Park[c,†], Jehan Kim[d,†], Geunjin Kim[a,b], Kilho Yu[a,b], Jinho Lee[a,b], Yong-Ryun Jo[a], Bong-Joong Kim[a], Hongkyu Kang[a,b], Junghwan Kim[a,b], Heejoo Kim[b,*] and Kwanghee Lee[a,b,*]

Processing additives have been widely utilized for high-performance organic bulk-heterojunction (BHJ) photovoltaic devices. However, the role of processing additives remained unclear due to the limited information relying on the final BHJ film state rather than the intermediate film state during solvent evaporation. Here, by using in-situ GIWAXS measurement on the intermediate BHJ film, we propose a possible phase separation mechanism in efficient BHJ solar cells consisting of a narrow band gap polymer (P1) and $PC_{71}BM$ via the use of 1-chloronaphthalene (1-CN) as a processing additive. We found that adding small amounts of an additive, 1-CN, with a high boiling point and a high $PC_{71}BM$ solubility can prolong the solvent evaporation time and dissolve many $PC_{71}BM$ molecules, promoting the strong P1 polymer:solvent and $PC_{71}BM$:solvent interaction to produce pure domains of each component. Thus, the bi-continuous networks for both P1 and $PC_{71}BM$ and their enlarged interfacial area are well fabricated in the BHJ films, inducing balanced photo-charge carrier densities for the electrons and holes and improving the overall photovoltaic performance. Therefore, our findings elucidate the kinetic motions of two organic phases affected by the physical properties of the solvents in the process of film formation and establish criteria for BHJ systems.

## Introduction

Bulk-heterojunction (BHJ) polymer solar cells (PSCs) composed of conjugated polymer donors and fullerene acceptors have attracted significant interest as promising renewable energy conversion devices because of their potential for manufacturing cost-effective, light-weight, flexible, and large-scale solar panels via solution process.[1-3] To achieve high power conversion efficiency (PCE) in BHJ solar cells, during recent decades, significant effort has been devoted to the design of push-pull type π-conjugated polymers (π-CPs), which have narrow band gaps with excellent charge mobility. As a result, recent reports showed high PCEs exceeding 10%,[4,5] which mostly involve hierarchical three phase structures: pure fullerene domains, pure π-CPs domains and π-CPs/fullerene inter-mixed domains.[6-8] Those excellent device performances are attributed to 1) nanoscale π-CPs/fullerene inter-mixed domains with large interfacial area, 2) efficient charge separation at the phase boundary, and 3) subsequent charge transport along continuous percolation paths (pure domains) to the corresponding electrode.[9,10] However, the composites of π-CP and fullerene derivatives frequently exhibit undesirable large phase segregation on the order of a few hundred nanometers, which is greater than the exciton (electron-hole pair) diffusion length (approximately 5-10 nm) of π-CPs,[11-13] thereby hindering efficient charge generation and transport in the BHJ films.[13-15] Furthermore, depending on their chemical structure of conjugated polymers, fullerene derivatives are often intercalated into polymer crystalline domains, producing a bimolecular crystal structure where the charge transport is severely limited.[16-18] Because the reduction of the large-scale phase segregation and bimolecular structure in BHJ film have been desired to ensure highly efficient PCE,[18-20] it is of great interest to fabricate the well-phase separation between polymers and fullerenes in the BHJ composites via various device fabrication techniques such as thermal annealing, solvent vapor annealing, processing additives.

To fabricate a desirable nanoscale phase separation in solution-processed BHJ solar cells, recently, the processing additive (PA) technique has been utilized, which consists of

simply adding a small volume of various high-boiling-point solvent additives such as 1-chloronaphthalene (1-CN) to BHJ blend solutions[21,22]. Because of the excellent solubility of each component in 1-CN, the PA technique can lead to a well-separated nano-morphology in the BHJ film.[23-26]

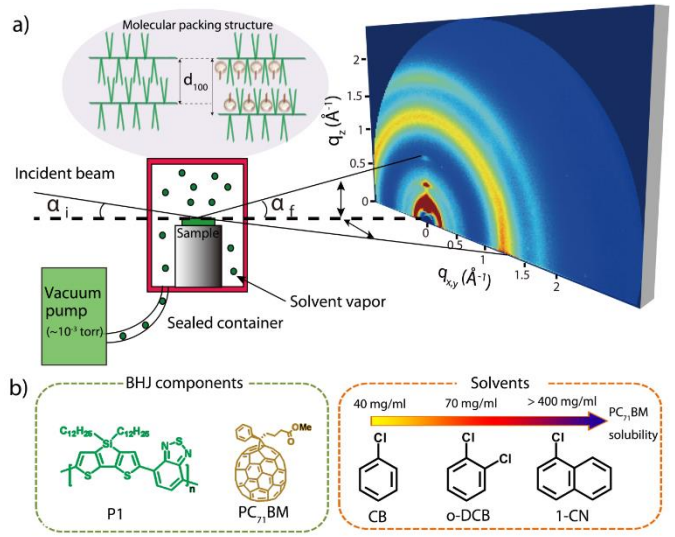


**Fig. 1.** a) Schematic image of the experimental setup for in-situ GIWAXS and x-ray reflectometry of thin film under a controlled film drying system. b) Chemical structures of P1 polymer, $PC_{71}BM$, chlorobenzene (CB), 1,2-dichlorobenzene (o-DCB) and 1-chloronaphthalene (1-CN), including $PC_{71}BM$ solubility.

However, considering the high b.p. of 1-CN compared with the host solvent, the solubility in 1-CN was insufficient to address the subsequent structural/morphological change during the transition from solution to solid film. Therefore, some issues are raised: 1) whether and how the use of additives can contribute to manipulating the molecular packing condition and phase separation of BHJ components and 2) whether and how controlling the solvent boiling point over the course of the solution process can also offer possible routes for reducing the bimolecular structure within BHJ film.[18] To clarify these issues, it is essential to investigate the molecular packing dynamics of push-pull type π-CPs and fullerene derivatives induced by 1-CN processing additives. However, so far, these studies have not been fully investigated despite their importance for correctly understanding the molecular packing and phase separation mechanism of BHJ components via processing additives.

In this contribution, by utilizing *in-situ* grazing incidence wide angle x-ray scattering (*in-situ* GIWAXS) measurement (**Figure 1a**), we investigate the effect of 1-CN on the structural/morphological evolution and mechanistic details of nanoscale phase separation in BHJ films consisting of poly[(4,4-didodecyldithieno[3,2-b:2',3'-d]silole)-2,6-diyl-alt-(2,1,3-benzothiadiazole)-4,7-diyl] (P1) and [6,6] phenyl-C71-butyric acid methyl ester ($PC_{71}BM$) (**Figure 1b**, left panel). The BHJ films were prepared from blends of chlorobenzene (CB, b.p. of approximately 131 ℃) with and without 4 % 1-CN (b.p. of approximately 265 ℃) by volume, as reported in the previous literature.[27] Additionally, to probe the correlation between the physical properties of solvents for BHJ blend solutions, such as solubility, boiling point, and molecular packing structure, BHJ films were also fabricated from neat 1,2-dichlorobenzene (DCB) (b.p. of approximately 180 ℃) with and without 4 % (v/v) 1-CN under the same conditions (**Figure 1b**, right panel).

As a result, we found that P1 has a strong tendency to form lamellar stacking, alternating side chains up and down along the polymer backbone in their crystallites. Because this structure can offer sufficient spaces for intercalation of $PC_{71}BM$ molecules, the formation of bimolecular crystal structures in BHJ films can be expected (**Figure 1a** in a shaded ellipse).[20] However, we observed that adding a small amount of 1-CN to the CB blend significantly decreases the fraction of bimolecular interaction and prevents the large-scale aggregation of $PC_{71}BM$, improving P1 crystallinity. In addition, it is observed that the BHJ films cast from high b.p. solvents such as DCB and DCB+1-CN blends also exhibited almost identical behaviours to those of the CB+1-CN blend. These results are confirmed by transmission electron microscopy (TEM) and current-voltage (*J-V*) characteristics, indicating that the morphological transition was induced by 1-CN and/or DCB solvent toward continuous percolation for the hole/electron path, leading to a dramatic increase in current density. Consequently, the BHJ solar cells processed with CB+1-CN, DCB, and DCB+1-CN blends exhibited similar PCE values of 4.6%, which is increased by more than 64% compared with the BHJ solar cells from the CB blend (PCE of 2.9%).

## Experimental methods

### Synthesis of material and solution preparation.

P1 polymers were synthesized following a previously published procedure. For this study, the number average molecular weight ($M_n$) and polydispersity index (PDI) of the specific P1 sample were 34 kDa and 2.4, respectively. The solutions of pristine materials, P1 and $PC_{71}BM$ (Nano C, > 99 %), were dissolved in anhydrous CB (Sigma Aldrich) at a concentration of 10 mg/ml and then maintained in an $N_2$ glove box. The solutions were heated to 100 ℃ with stirring for 3 days to ensure complete dissolution of the materials. For the BHJ solution, P1 polymer and $PC_{71}BM$ were dissolved in 1 ml of solvents such as CB and/or DCB at a 1:1 ratio (10 mg: 10 mg). For the processing additive, 1-CN (Alfa Aesar >98 %) was added to the BHJ solutions in CB and DCB at a concentration of 4 % by volume. All solutions were prepared in an $N_2$-filled glove box.

### *In-situ* GIWAXS measurements.

Grazing-incidence wide-angle X-ray scattering (GIWAXS) measurements were performed in real time at the 3C-SAXSl beam line in the Pohang Accelerator Laboratory (PAL) using a monochromatized X-ray radiation source of 10.55 eV (λ = 0.117 nm) and a two-dimensional (2-D) charge-coupled device (CCD) detector (Mar165 CCD). The BHJ blend solutions with

various solvent systems were deposited on Si substrates, and the as-prepared samples were mounted on a z-axis goniometer equipped with a vacuum chamber (~$10^{-3}$ torr; 1 torr ~ 133 Pa). The samples were 0.201 m away from the CCD detector. The incident angle of each X-ray beam was set as 0.14° (substrate critical angle), and the scattering angles were determined from the positions of the reflected X-ray beam from the silicon substrate using pre-calibrated silver behenate. The measurements of each sample were conducted every 5 minutes for 40 minutes to approach the final film state.

**TEM measurements.**

Top-down TEM images of the sample films were recorded using a Tecnai G2 F30 S-Twin microscope operated at an acceleration voltage of 300 kV. The sample films for TEM measurement were obtained by peeling the pre-deposited film (*t* ≈ 70 nm) from a glass substrate, and the films were transferred onto 200 mesh copper grids with carbon film (Electron Microscopy Sciences).

**Device fabrication.**

Indium tin oxide (ITO)-coated glass substrates with a sheet resistance of ~15 ohm/sq were cleaned by sequentially ultrasonicating the material with detergent, deionized water, acetone, and isopropanol. The substrates were then dried for 1 hour in an oven. Poly(3,4-ethylenedioxythiophene):poly(styrensulfonate) (PEDOT:PSS, Al 4083) was spin-coated onto the ITO-coated glass substrate to obtain a layer with a thickness of 25 nm and baked for 10 min at 140 °C in air. After transferring into a $N_2$-filled glove box, the blend solutions were spin cast on top of the PEDOT:PSS layer. The thickness of the BHJ films was controlled to ca. 120 ~ 135 nm, which was measured using a Surf-corder ET-3000 (Kosaka Laboratory Ltd.), and they were dried at 70 °C for 1 hour to completely remove the residual solvent. For all of the devices, an aluminium electrode with a thickness of 100 nm was thermally deposited under vacuum ($10^{-7}$ torr).

**Calibration and measurement.**

The spectrum obtained from the Xenon (Xe) lamp (300 W Oriel) of a solar simulator was calibrated using a calibrated standard silicon solar cell with a protective window made from a KG5 filter glass produced by the National Renewable Energy Laboratory (NREL). The current-voltage (*J-V*) characteristics of the devices were measured using a Keithley 236 SMU, and simulated 100 mW/cm$^2$ sunlight from the calibrated Xe lamp was employed. In the measurements, an AM 1.5-G filter was utilized under a $N_2$ atmosphere.

## Results and discussion

***In-situ* observation of molecular packing motif in P1:$PC_{71}BM$ BHJ films fabricated from various solvent systems.**

The structural evolution in BHJ systems during drop-cast and solvent evaporation was carefully investigated in real time using GIWAXS measurement with a dedicated experimental setup (**Figure 1a**). The 2-dimensional (2D) GIWAXS patterns of the P1:$PC_{71}BM$ blends were obtained every 5 minutes after drop-casting on silicon substrate under vacuum of ~$10^{-3}$ torr at critical angle (see supporting information, **Figure S1** and **Figure S2**). **Figure 2a-d** show out-of-plane GIWAXS profile plots of BHJ films from CB, CB+1-CN, DCB and DCB+1-CN solvents, respectively. For clarity, the GIWAXS patterns of the BHJ films and pristine P1 polymers obtained by spin-coating procedure are also shown in Supporting Information, **Figure S3** and **S4**, respectively.

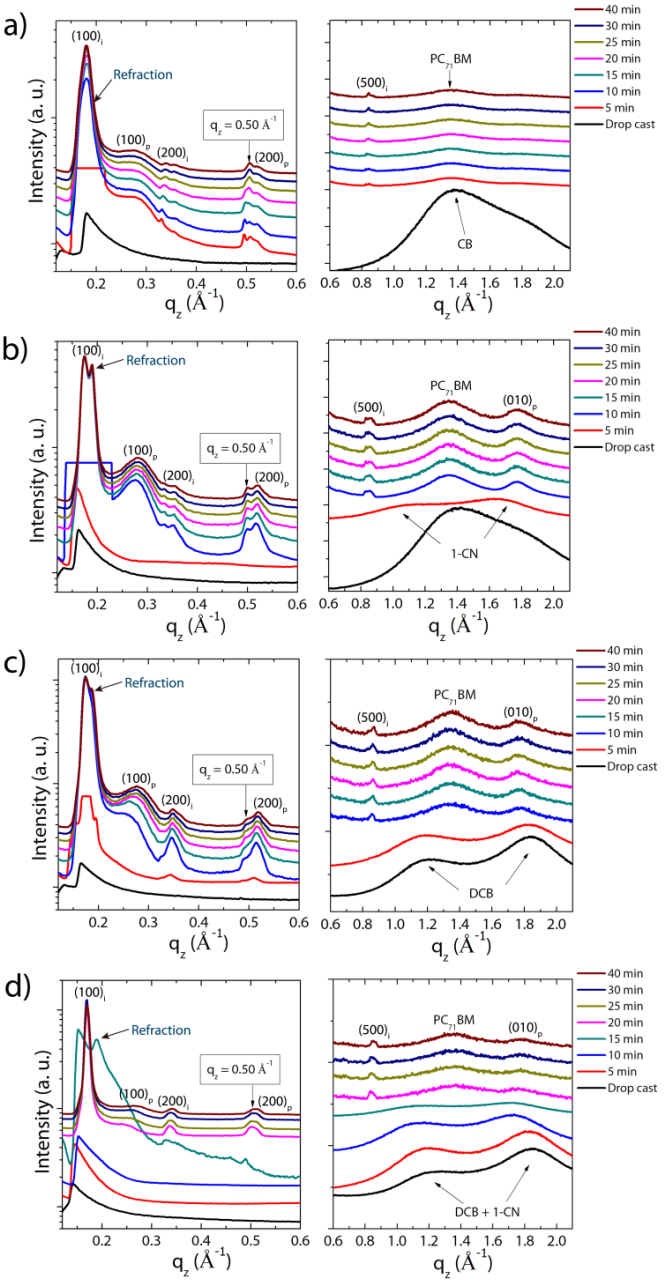

**Fig. 2.** Profile plots of real-time GIWAXS at increasing film drying times, showing the emergence of the diffraction pattern of P1 polymer (h00), $PC_{71}BM$ and the disappearance of the diffraction pattern of various solvents on Si substrate (log scale left, linear scale right). a) Neat CB solvent. b) CB+1-CN solvent. c) Neat DCB solvent. d) DCB+1-CN solvent. All diffraction patterns were obtained at substrate critical angle ~ 0.14°.

All BHJ samples regardless of solvent and fabrication procedure showed a new crystal peak at $q_z$ = 0.18 Å$^{-1}$ at increasing drying times, which is associated with a lamellar spacing ($d$) of the $(100)_i$ plane ($d$ = 2π/0.18 Å$^{-1}$ = 34.9 Å), whereas the pristine P1 polymer film shows a diffraction peak at $q_z$= 0.28 Å$^{-1}$ corresponding to a lamellar spacing of the $(100)_p$ plane ($d$ = 2π/0.28 Å$^{-1}$ = 22.4 Å).[28] These results indicated that $PC_{71}BM$ intercalates into P1 polymer crystallite to form a P1:$PC_{71}BM$ bimolecular crystal structure due to sufficient space between the alkyl side chains along the polymer backbone (the subscripts "i" and "p" denote intercalated bimolecular structure and pristine P1 polymer, respectively). The split peaks of BHJ samples at $q_z$ = 0.18 Å$^{-1}$ were obtained by an effect of refraction beam (see detail information in supporting information, Figure S5). Furthermore, all BHJ films from various solvent systems also have a $(100)_p$ Bragg peak from pristine polymer at $q_z$ = 0.28 Å$^{-1}$ crystallites, which means that all BHJ films studied here are mixtures of bimolecular and non-bimolecular phases.

In general, the spin-casting procedure would show different drying dynamics of solvents from that of the drop-casting procedure due to kinetic trapping caused by external forces and relatively fast drying time during spin coating.[29] However, it is worthy to note that by comparing BHJ films with various solvent systems obtained from spin-casting and drop-casting, similar trends of GIWAXS patterns are observed from the both procedures: an increasing intensity of $(100)_p$ for the lamellar stacking of pure polymer domains and a decreasing bimolecular peaks $(100)_i$ as the boiling point of solvent is increasing (see Figure S3). To exploit the more possible and precise molecular packing dynamics and/or phase separation, it would be considered to investigate the more thermodynamically controlled regimes by minimizing the kinetic trapping effect as a function of drying time. Thus, we clearly found that the trends for increasing polymer lamellar peak were observed upon increasing drying times via the drop-casting procedure with the use of high-boiling-point solvents such as CB+1-CN, DCB, DCB+1-CN, whereas those for CB solvent decreases in the same time interval (**Figure 2a-d**, left panels). In addition, we observed the in-situ formation of bimolecular crystal structure of the BHJ samples during drop-casting as evidenced by the presence of a diffraction peak at $q_z$ = 0.50 Å$^{-1}$. The peaks are only obtained from the intercalated blend system because of the ordered arrangement of fullerene derivatives in the lamellar layer of P1. As expected in the change of polymer lamellar peak, the intensity of the peaks at 0.50 Å$^{-1}$ from CB+1-CN, DCB and DCB+1-CN decrease with increasing film drying time, whereas the intensity from the CB blend is rather enhanced. In particular, the amount of reduction of the peak at 0.50 Å$^{-1}$ is greater in the following order: DCB+1-CN > DCB > CB+CN > CB, which is similar to the order of solubility of $PC_{71}BM$ and the order of the boiling points of the solvents. Similar trends are observed in the reduction of the intense $(700)_i$ peak in the in-plane direction depending on the order of the boiling points of the solvents,[20] which might be related to the distance between the polymer backbone and intercalated $PC_{71}BM$ even though the origin of this intense $(700)_i$ peak has not been clearly understood (see Supporting Information, **Figure S6**).[30]

As a consequence of those features, an amorphous $PC_{71}BM$ halo ($q_z$ = 1.3 Å$^{-1}$) phase is shown in the GIWAXS spectra of films cast from CB+1-CN, DCB and DCB+CN (**Figure 2b-d**, right panels).[10] Therefore, it can be suggested here that to avoid the unfavourable BHJ structure, a good solvent for $PC_{71}BM$ is an essential prerequisite, and the boiling point should be higher than CB. Another interesting feature is the strong $(010)_p$ Bragg peak at $q_z$ = 1.74 Å$^{-1}$ ($d$ = 2π/1.74 Å$^{-1}$ = 3.61 Å) in 1D GIWAXS patterns from CB+1-CN, DCB and DCB+1-CN upon enhancing the out-of-plane π-π stacking of P1 polymer, which would provide a continuous percolation path for efficient hole transport along the vertical direction from the BHJ to the electrode. For the CB solvent, however, the out-of-plane $(010)_p$ Bragg peak was not detected, implying that it is unlikely for the significant charge carrier flow in the vertical direction to be as pronounced as others (**Figure 2a**, right panel).

As the broad diffraction pattern of residual solvents from $q_z$ = 0.8 Å$^{-1}$ to $q_z$ = 2.0 Å$^{-1}$ in the profiles could be considered the interference of solvent molecules by the grazing incident light, we were able to determine the onset of the falling-rate drying period in terms of the boiling point of the solvent. For the CB solvent (b.p. ~135 ℃), an infinitesimal intensity of the $PC_{71}BM$ amorphous peak (**Figure 2a**, right panel) was observed within 5 minutes after drop casting, and the intensity of the amorphous peak did not change for 35 minutes. The low intensity of the $PC_{71}BM$ peak may be attributed to the formation of bimolecular structure and/or large ordered aggregated domains of $PC_{71}BM$. However, by using CB+1-CN or DCB solvent (b.p. ~ 180 ℃), the $PC_{71}BM$ amorphous peak (**Figure 2b** and **Figure 2c**, right panel) was significantly enhanced at approximately 10 minutes, whereas for DCB+1-CN (b.p. > 180 ℃), it was even more delayed, taking up to 20 minutes for the enhanced peak to appear (**Figure 2d**, right panel). Accordingly, the strong intensity of the $PC_{71}BM$ amorphous peak in the subsequent profiles may be attributed to the well-dispersed $PC_{71}BM$ domains within BHJ morphology by using good solvents, such as DCB and a small amount of 1-CN, which clearly suppress the growth of bimolecular phases as mentioned above. Therefore, it is worth re-emphasizing here that to obtain the desirable BHJ morphology, a good solvent for the BHJ components is crucial, and a high-boiling-point additive is essential to provide enough time for the complete film formation. This point is consistent with the criteria for seeking potentially useful additives for highly efficient organic photovoltaic cells, which have been described in the previous literature.[23]

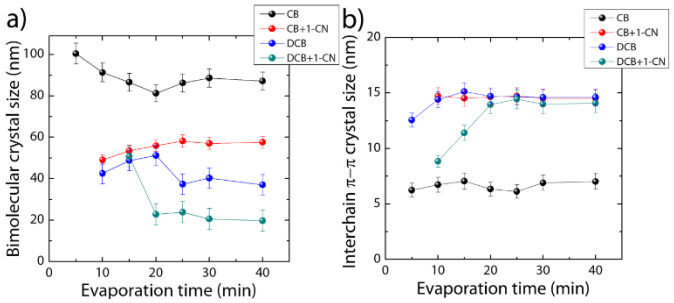


**Fig. 3.** a) Plots of bimolecular crystal size in the P1:$PC_{71}BM$ BHJ films under a controlled solvent drying system as a function of film drying time, as obtained from the emergence of an out-of-plane peak at qz =0.50 $Å^{-1}$. b) Plots of interchain π-π crystals in P1:$PC_{71}BM$ BHJ films under a controlled solvent drying system as a function of film drying time, as obtained from the emergence of an in-plane peak at $q_{x,y}$ =0.26 $Å^{-1}$. The error bars represent standard deviations derived from more than three samples.

To clearly demonstrate the suppression of the bimolecular phase in the BHJ systems by high-boiling-point processing additives, we monitored the size of the bimolecular crystallite in BHJ films processed with various solvents as a function of solvent evaporation time. The sizes of the crystallites were calculated using the Sherrer equation with full width at half maximum (FWHM) of the out-of-plane peaks at $q_z$ =0.50 $Å^{-1}$ (**Figure 3a**). As seen in **Figure 3a** (black solid circles and line), the BHJ films from the CB solvent exhibit quite large bimolecular crystal sizes ranging from 100 nm to 85 nm as a function of drying time. However, the BHJ films from CB+1-CN (**Figure 3a**, red solid circles and line) show the crystal size reduced to ~55 nm without further significant change for 40 minutes. Significant reductions in the bimolecular crystal size were observed in the BHJ films from DCB and DCB+1-CN solvents (**Figure 3a**, blue and dark cyan circles and line): 30 nm for DCB and 20 nm for DCB+1-CN solvent at the final film stage. It is further noted that the various solvents simultaneously influence the crystalline domain size of P1 polymer with respect to interchain π-π ordering along the substrate surface (face-on structure). The effects of various solvents on the crystalline size of P1 polymer in the BHJ films were also investigated, as shown in **Figure 3b**. In the BHJ films from neat CB, the small size (~5 nm) of the crystallites for P1 polymer was observed at the final film stage, whereas the BHJ films from CB+1-CN, neat DCB and DCB+1-CN solvent exhibited the enlarged size of ~15 nm in the same regimes, which is threefold higher than in neat CB solvent. This result provides evidence that solvents with high boiling point and high $PC_{71}BM$ solubility (here, DCB and 1-CN) weaken the molecular interaction between P1 polymer and $PC_{71}BM$. Therefore, the formation of bimolecular structure was suppressed by minimizing the intercalation of $PC_{71}BM$ molecules into the polymer lamellar self-assembly. As a result, the BHJ phase separation can be improved during film formation by physically adding such an additive to the parent solvent.

**Evolved nano-morphology of P1:$PC_{71}BM$ BHJ films by various solvent systems.**

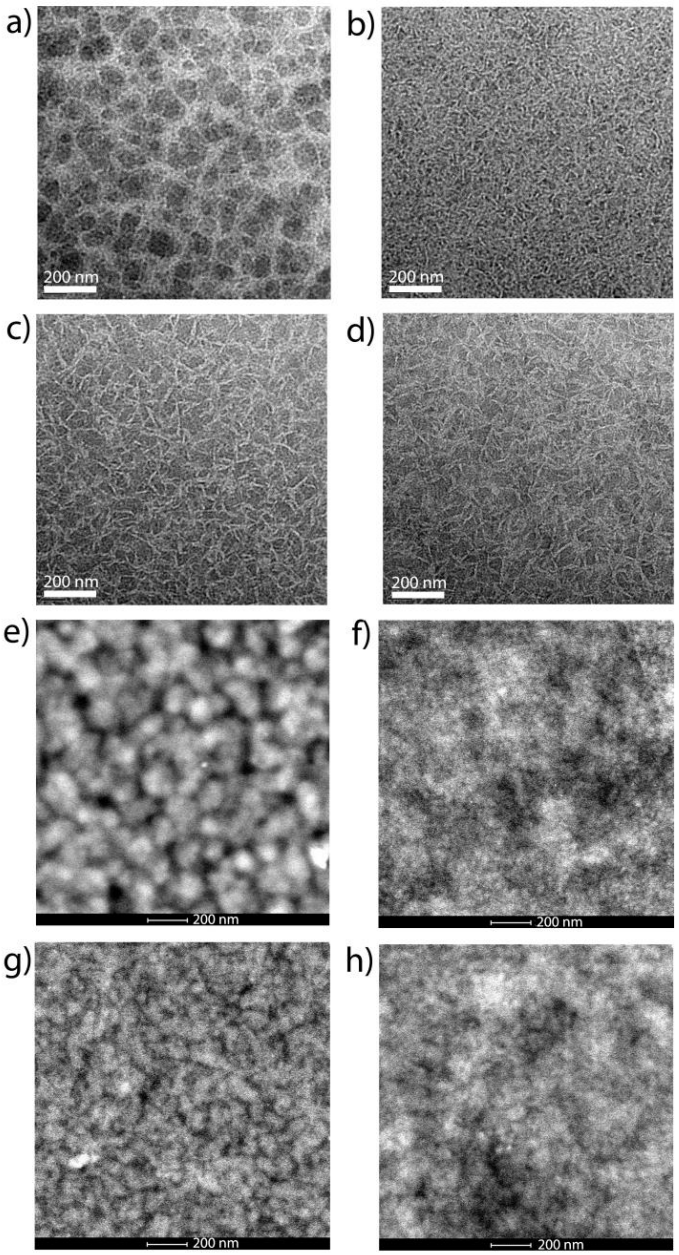


**Fig. 4.** Top-down TEM images of P1 polymer:$PC_{71}BM$ BHJ film: a) CB solvent; b) CB+1-CN solvent; c) DCB solvent; d) DCB+1-CN solvent. HAADF-STEM images of the corresponding P1 polymer:$PC_{71}BM$ BHJ film: e) CB solvent; f) CB+1-CN solvent; g) DCB solvent; h) DCB+1-CN solvent.

We observed the evolved nano-scale morphology of P1:$PC_{71}BM$ BHJ films from various solvents using top-down transmission electron microscopy (TEM) measurement, as shown in **Figure 4a-d**. High-angle annular dark-field scanning transmission electron microscopy (HAADF-STEM) was simultaneously on the corresponding nanomorphology of BHJ

films (see **Figure 4e-h**). In general, the HAADF-STEM images are obtained from incoherently scattered electrons, and the electrons emitted from the electron gun are highly sensitive to the relative differences in the electron density of the samples.[31] Thus, the brighter regions observed in the HAADF-STEM images can be attributed to the relatively higher electron density of the $PC_{71}BM$ region compared with the P1 polymer region. As shown in the TEM image of the BHJ films from neat CB solvent (**Figure 4a**), the formation of large $PC_{71}BM$ aggregation with an average diameter of ~200 nm was observed. The HAADF-STEM image of the corresponding morphology in Figure 4e confirms that the $PC_{71}BM$ domains are significantly discontinuous by the boundary region, which might be filled with pristine P1 polymers and/or bimolecular structures. However, this discontinuity was significantly reduced in the BHJ films processed with CB+1-CN, as shown in the TEM and HAADF-STEM images (Figure 4b and 4f): a smooth and uniform morphology was observed without any $PC_{71}BM$ aggregation. In addition, new fibril structures of pristine P1 polymer have emerged and are fully interconnected, which is consistent with the enhanced out-of-plane π-π stacking of P1 polymer as measured in the in-situ GIWAXS measurement. We also found that the TEM images of BHJ films from DCB and DCB+1-CN solvent (Figure 4c,g and 4d,h, respectively) have a similar uniform morphology with an interconnected fibril structure of P1 polymers and a slight difference in $PC_{71}BM$ distribution. We speculate that the difference in $PC_{71}BM$ solubility in DCB (~70 mg/ml) and 1-CN (> 400 mg/ml) solvent would induce the different $PC_{71}BM$ distribution in the BHJ film.

**Optoelectric characterizations in P1 polymer:$PC_{71}BM$ BHJ films fabricated from various solvent systems.**

The photovoltaic performances from different solvent systems were probed by fabricating a series of solar cells prepared by spin-coating P1:$PC_{71}BM$ BHJ films onto glass/ITO/poly(3,4-ethylenedioxythiophene):poly(styrenesulfonate) substrates. The thickness of the BHJ films was controlled to 130 ± 10 nm. Then, an aluminium cathode was deposited by thermal evaporation, resulting in a final thickness of approximately 100 nm. A schematic of the final device structure is shown in **Figure 5a**. The solar cells were empirically optimized by evaluating variations in the thickness and utilizing thermal treatments (see Supporting Information, **Figures S7** and **S8**). **Figure 5b** shows the *J-V* characteristics of the corresponding devices fabricated from various solvent systems under AM 1.5-G irradiation at 100 mW/cm$^2$. The BHJ devices produced from the blend in neat CB (**Figure 5b**, black line) with optimized thickness (approximately 110 nm) had a PCE of 2.9 % with a short-circuit current density ($J_{sc}$) of 9.3 mA/cm$^2$, an open-circuit voltage ($V_{oc}$) of 0.58 V, and a fill factor (FF) of 0.53. The low $J_{sc}$ value can be attributed to the small BHJ interfacial area with the large-scale phase separation. By contrast, the device fabricated from CB+1-CN (**Figure 5b**, red line) had an enhanced $J_{sc}$ of 15.7 mA/cm$^2$, a $V_{oc}$ of 0.59 V, and an FF of 0.48. Moreover, the devices fabricated from neat DCB and DCB+1-CN (**Figure 5b**, blue line and dark cyan line) exhibited almost identical device performances to the devices fabricated from CB solvent containing 1-CN (see more detail performance values in Supporting Information, **Tables S1** and **S2**). These results are in agreement with the results of in-situ GIWAXS and TEM measurements.

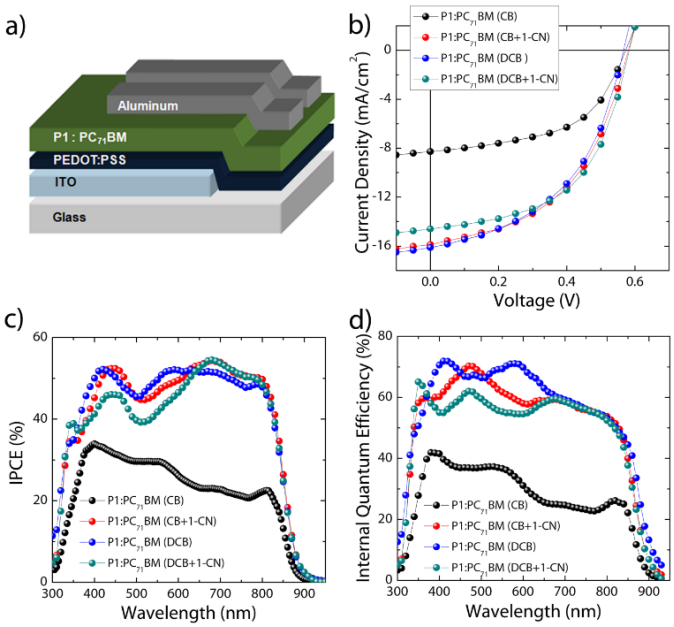


**Fig. 5.** a) Schematic presentation of the device structure of P1:$PC_{71}BM$ solar cells, b) the *J-V* characteristics, c) the IPCE characteristics, and d) the calculated IQE characteristics of the corresponding devices using CB, CB+1-CN, DCB, and DCB+1-CN solvents.

**Figure 5c** shows the incident photon-to-charge carrier efficiency (IPCE) spectra of the corresponding devices. The $J_{sc}$ values obtained by integrating the IPCE spectra are consistent with the measured $J_{sc}$ values under the same conditions (within 4 % error). Note that the IPCE values of all devices except the device with CB solvent exhibited a dramatic increase in the wavelength range from 920 nm to 650 nm, which exactly overlapped with the optical absorption spectrum of P1 polymers (see Supporting Information, **Figure S9a**). As observed in the GIWAXS measurements, these enhancements in the IPCE spectra are most likely related to the significant reduction of bimolecular structure and enhanced π-π interaction along the pathway of the P1 polymer through the BHJ layer. Hence, the improved current density in the devices processed with CB+1-CN, DCB, and DCB+1-CN can be attributed to the formation of continuous percolating pathways of P1 polymer through the BHJ layer rather than $PC_{71}BM$ self-assembly. This result is also supported by the observation of the interconnected P1 polymer fibril structure in TEM measurement.

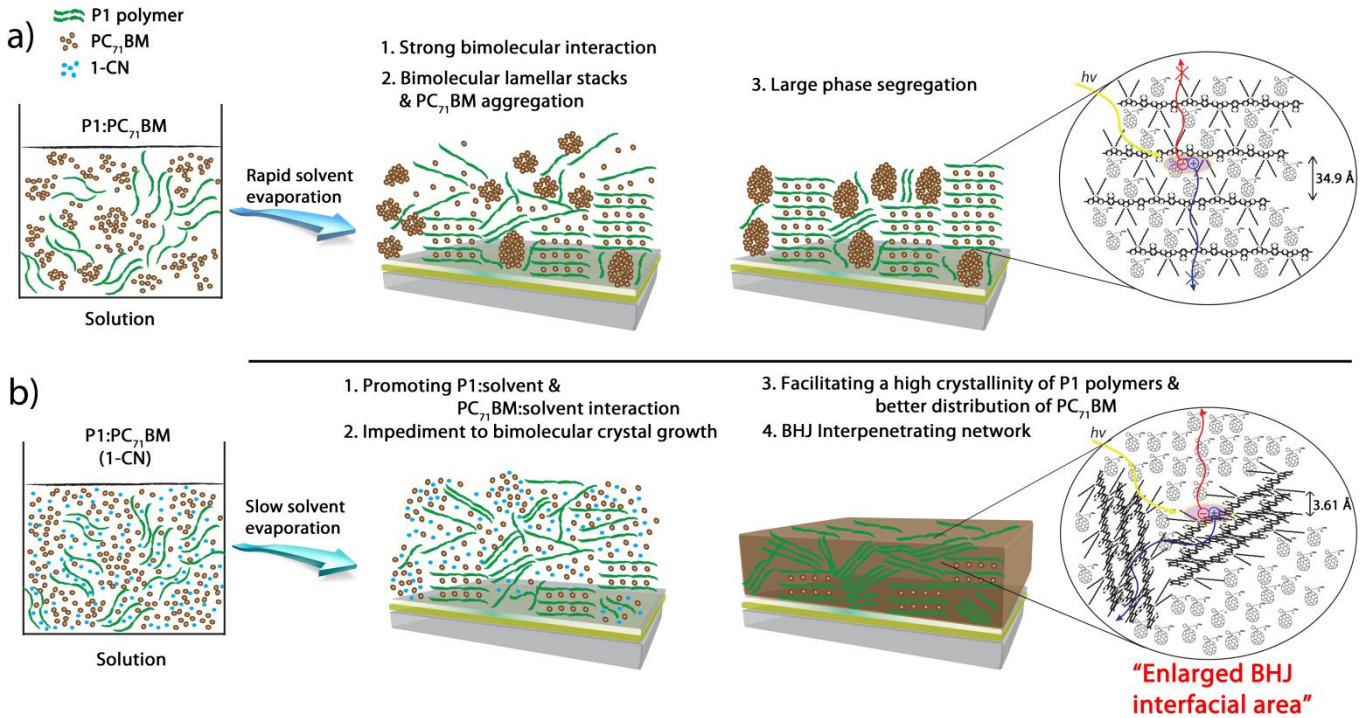


**Fig. 6.** Schematic illustrations show the stages of the molecular packing motif of P1:$PC_{71}BM$ BHJ blends with and without 1-CN solvent during the film formation. Green lines represent P1 polymers, brown dots are $PC_{71}BM$ molecules, and cyan dots are 1-CN solvent molecules. Inset figures display the molecular packing structure of P1 polymers and $PC_{71}BM$ with expected charge separation and transport process.

To further analyse the efficient charge separation and collection upon the improved percolation pathway, the internal quantum efficiency (IQE) spectra were calculated using the following equation:

$$\mathrm{IQE}\ (\lambda) = \frac{\mathrm{IPCE}\ (\lambda)}{\mathrm{Abs}\ (\lambda)} \qquad (1)$$

where Abs (λ) is the amount of absorption of the active layer along the wavelength.[9,32] As shown in **Figure 5d**, the devices developed from neat CB exhibited a relatively lower IQE (%) in the overall wavelength range from 920-300 nm. By contrast, high IQE values approaching ~ 70% were observed in the devices fabricated from CB+1-CN, neat DCB, and DCB+1-CN solvents at the specified wavelength range, indicating that 70% of photo-generated charge carriers can be effectively collected at the electrode through the improved BHJ morphology. In addition, it is noticeable that the IQE values of the devices with CB+1-CN, neat DCB, and DCB+1-CN in the range of 920-650 nm, which are attributed to the P1 polymer, were almost identical for each device, whereas a little fluctuation was observed in the short wavelength range (approximately 650-300 nm), which might be related to a changed electric field distribution within the BHJ films[27] and/or a slight reduction of the amount of $PC_{71}BM$ within the films due to enhanced solubility by 1-CN during spin-casting procedure (see Supporting Information, **Figure S9b**). As observed in the HAADF-STEM analysis, these similar IQE spectra for the devices processed with CB+1-CN, DCB, and DCB+1-CN can be attributed to the improved P1 polymer network and $PC_{71}BM$ distribution without an aggregation. Therefore, from this series of experimental results, it can be concluded that the percolation path along P1 polymers and the enlarged interfacial area in the BHJ films can be achieved by using solvents with high boiling points and high $PC_{71}BM$ solubility.

**Proposed molecular packing mechanism of P1:$PC_{71}BM$ BHJ film via various solvent systems.**

Based on our observations, we summarize the possible mechanism for the morphologic formation in the P1:$PC_{71}BM$ BHJ composite system with 1-CN processing additive incorporated as described in the schematic illustration (**Figure 6**). For the BHJ film without 1-CN solvent (**Figure 6a**), the P1 polymers and $PC_{71}BM$ are assembled to produce the bimolecular structure because the intermolecular stacking of P1 and the aggregation of $PC_{71}BM$ are rapidly facilitated due to the relatively fast evaporation of the solvent. During this process, some portion of stabilized $PC_{71}BM$ would be situated between P1 polymer chains (lamellar direction). As a result, the formation of bi-continuous interpenetrating networks in the BHJ films is hindered, leading to reduced charge generation and transport in the BHJ solar cells.[19] However, the addition of 1-CN to the BHJ mixtures (**Figure 6b**) allows a change in the kinetics to promote the formation of film growth by the following rationale; the high boiling point and high $PC_{71}BM$ solubility of 1-CN can elongate the solvent evaporation time

and dissolve many $PC_{71}BM$ molecules even in the bimolecular structure, producing a strong P1 polymer:solvent interaction and $PC_{71}BM$:solvent interaction. This process can prevent the formation of bimolecular structure and facilitate the high crystallinity of the P1 polymer and better distribution of the $PC_{71}BM$ molecules, which lead to the bi-continuous charge carrier pathway with an enlarged interfacial area. Therefore, dramatic improvement in the device performance can be expected. Similarly, the mechanism of the 1-CN solvent could be applicable to the DCB solvent due to its similar properties, such as higher boiling point and higher $PC_{71}BM$ solubility than CB but less than 1-CN.

## Conclusion

The detailed kinetics of molecular packing behaviour in P1:$PC_{71}BM$ BHJ via the use of 1-CN processing additive in CB and DCB was investigated in real time using GIWAXS. Although P1 polymer has inherently less self-assembly ability than small molecules, the assembly can be expedited by fast drying solvent and by the intercalation of small molecules due to the strong affinity between P1 polymer and $PC_{71}BM$, which induce a bimolecular crystal structure and a large-scale phase aggregation of $PC_{71}BM$. Nonetheless, adding a small amount of 1-CN and using a good solvent, such as DCB for $PC_{71}BM$, significantly impede the formation of bimolecular structure and consequently lead to an enlarged interfacial area between P1 polymer and $PC_{71}BM$. This result could be attributed to the enhanced solubility of $PC_{71}BM$ for the extended film growth time with 1-CN and/or DCB solvent, which presumably causes a strong polymer:solvent and $PC_{71}BM$:solvent interaction instead of polymer:$PC_{71}BM$ intermoleculcar interaction. The series of further experimental results using the TEM, HAADF-STEM, and *J-V* characteristics clearly support that a bi-continuous network for both P1 and $PC_{71}BM$ with improved out-of-plane π-π orientation of the polymers forms well in the BHJ films fabricated from 1-CN and/or DCB solvent, exhibiting similar photo-charge carrier density for both the electrons and holes. In particular, it can be expected that such *in-situ* studies for the understanding of the molecular packing motif underlying the solvent effects of 1-CN and/or DCB can contribute rationales for elucidating the physical contribution of BHJ components to the phase separation mechanism with the use of processing additives, which is required for developing high-performance photovoltaic devices.

## Acknowledgements.

We thank Prof. G. C. Bazan at UCSB for providing materials and helpful information. We also thank the Heeger Center for Advanced Materials (HCAM) and the Research Institute of Solar & Sustainable Energies (RISE) at the Gwangju Institute of Science and Technology (GIST) of Korea for device fabrication and measurement. This work was supported by the National Research Foundation of Korea (NRF) grant, funded by the Korean government (MSIP) (NRF-2014R1A2A1A09006137). K. Lee also acknowledges support from the National Research Foundation of Korea (NRF) grant, which was funded by funded by the Korean government (MSIP) (No. 2008-0062606, CELA-NCRC).

## Notes and references

[a] School of Materials Science and Engineering, Gwangju Institute of Science and Technology, Gwangju 500-712, Korea
[b] Heeger Center for Advanced Materials (HCAM) & Research Institute for Solar and Sustainable Energies (RISE), Gwangju Institute of Science and Technology, Gwangju 500-712, Korea
[c] Departments of Chemistry, Hankuk University of Foreign Studies, Yongin 449-791, Republic of Korea
[d] Pohang Accelerator Laboratory (PAL), Pohang University of Science and Technology (POSTECH), Pohang 790-784, Republic of Korea
*Address correspondence to heejook@gist.ac.kr, klee@gist.ac.kr.

† S. Kwon, J. K. Park and J. Kim made equal contributions to this work (Co-first authors)

Electronic Supplementary Information (ESI) available: [Further details on the in-situ GIWAXS measurements as well as additional information on the *J-V* characteristics of the investigated P1:$PC_{71}BM$ BHJ films]. See DOI: 10.1039/b000000x/

1. G. Yu, J. Gao, J. C. Hummelen, F. Wudl, A. J. Heeger, *Science* 1995, **270**, 1789.
2. D. Mühlbacher, M. Scharber, M. Morana, Z. Zhu, D. Waller, R. Gaudiana, C. J. Brabec, *Adv. Mater.* 2006, **18**, 2884.
3. F. C. Krebs, T. Tromholt, M. Jorgensen, *Nanoscale* 2010, **2**, 873.
4. C. E. Small, S. Chen, J. Subbiah, C. M. Amb, S. Tsang, T. Lai, J. R. Reynolds, F. So, *Nat. Photo.* 2012, **6**, 115.
5. Z. He, C. Zhong, S. Su, M. Xu, H. Wu, Y. Cao, *Nat. Photo.* 2012, **6**, 591.
6. M. Su, C. Kuo, M. Yuan, U. Jeng, C. Su, K. Wei, *Adv. Mater.*, 2011, **23**, 3315.
7. C. Liu, Y. Su, J. Jiang, H. Chen, S. Lin, C. Su, U. Jeng, K. Wei, *J. Mater. Chem. A*, 2014, **2**, 20760.
8. Y. Su, C. Liu, J. Jiang, C. Tsao, H. Cha, U. Jeng, H. Chen, K. Wei, *J. Phys. Chem. C*, 2015, **119**, 3408.
9. S. H. Park, A. Roy, S. Beaupré, S. Cho, N, Coates, J. S. Moon, D. Moses, M. Leclerc, K. Lee, A. J. Heeger, *Nat. Photo.* 2009, **3**, 297.
10. B. Schmidt-Hansberg, M. Sanyal, M. F. G. Klein, M. Pfaff, N. Schnabel, S. Jaiser, A. Vorobiev, E. Müller, A. Colsmann, P. Scharfer, D. Gerthsen, U. Lemmer, E. Barrena, W. Schabel, *ACS Nano* 2011, **5**, 8579.
11. A. Haugeneder, M. Neges, C. Kallinger, W. Spirkl, U. Lemmer, J. Feldmann, U. Scherf, E. Harth, A. Gugel, K. *J. Phys. Rev. B* 1999, **59**, 15346.
12. M. Theander, A. Yartsev, D. Zigmantas, V. Sundstrom, W. Mammo, M. R. Andersson, O. Inganas, *Phys. Rev. B* 2000, **61**, 12957.
13. J. E. Kroeze, T. J. Savenije, M. J. W. Vermeulen, J. M. Warman, *J. Phys. Chem. B* 2003, **107**, 7696.
14. C. H. Woo, P. M. Beaujuge, T. W. Holcombe, O. P. Lee, J. M. J. Frechet, *J. Am. Chem. Soc.* 2010, **132**, 15547.
15. J. S. Moon, C. J. Takacs, S. Cho, R. C. Coffin, H. Kin, G. C. Bazan, A. J. Heeger, *Nano Lett.* 2010, **10**, 4005.



 

16. N. C. Cates, R. Gysel, Z. Beiley, C. E. Miller, M. F. Toney, M. Heeney, I. McCulloch, M. D. McGehee, *Nano Lett.* 2009, **9**, 4153.
17. F. C. Jamieson, E. B. Domingo, T. McCarthy-Ward, M. Heeney, N. Stingelin, J. R. Durrant, *Chem. Sci.*, 2012, **3**, 485.
18. J. Liu, L. Chen, B. Gao, X. Cao, Y. Han, Z. Xie, L. Wang, *J. Mater. Chem. A*, 2013, **1**, 6216.
19. S. Nilsson, A. Bernasik, A. Budkowski, E Moons, *Macromol.* 2007, **40**, 8291.
20. N. C. Miller, S. Sweetnam, E. T. Hoke, R. Gysel, C. E. Miller, J. A. Bartelt, X. Xie, M. F. Toney, M. D. McGehee, *Nano Lett.* 2012, **12**, 1566.
21. R. C. Coffin, J. Peet, J. Rogers, G. C. Bazan, *Nat. Chem.* 2009, **1**, 657.
22. H. Liao, C. Ho, C. Chang, M. Jao, S. B. Darling, W. Su, *Mater. Today*, 2013, **16**, 326.
23. C. Hoven, X. Dang, R. C. Coffin, J. Peet, T. Nguyen, G. C. Bazan, *Adv. Energy Mater.* 2010, **22**, E63.
24. J. Jo, D. Gendron, A. Najari, J. S. Moon, S. Cho, M. Leclerc, A. J. Heeger, *Appl. Phys. Lett.* 2010, **97**, 203303.
25. J. Jo, A. Pron, P. W. Leong, J. D. Yuen, J. S. Moon, M. Leclerc, A. J. Heeger, *Adv. Energy Mater.* 2012, **2**, 1397.
26. J. K. Park, C. Kim, B. Walker, T. Nguyen, J. H. Seo, *RSC Adv.* 2012, **2**, 2232.
27. S. Kwon, J. K. Park, G. Kim, J. Kong, G. C. Bazan, K. Lee, *Adv. Energy Mater.* 2012, **2**, 1420.
28. Y. D. Park, J. K. Park, J. H. Seo, J. D. Yuen, W. H. Lee, K. Cho, G. C Bazan, *Adv. Energy Mater.* 2010, **1**, 63.
29. G. D. Luca, A. Liscio, M. Melucci, T. Schnitzler, W. Pisula, C. G. Clark, Jr, L. M. Scolaro, V. Palermo, K. Mullen, P. Samori, *J. Mater. Chem.*, 2010, **20**, 71.
30. A. C. Mayer, M. F. Toney, S. R. Scully, J. Rivnay, C. J. Brabec, M. Scharber, M. Koppe, M. Heeney, I. McCulloch, M. D. McGehee, *Adv. Funct. Mater.* 2009, **19**, 1173.
31. D. B. Williams, C. B. Carter, Transmission Electron Microscopy: a Textbook for Materials Science. Part 3: Imaging. Springer, New York, 2009, ch. **22**, pp. 371-381.
32. L. H. Slooff, S. C. Veenstra, J. M. Kroon, D. J. D. Moet, J. Sweelssen, M. M. Koetse, *Appl. Phys. Lett.* 2007, **90**, 143506.